

In-situ growth of $Zr_{1-0.5x}Cd_xW_2O_8$ on $ZrW_2O_8/CdWO_4$ manufactured by electron beam irradiation with superior photocatalytic activity for degradation of tetracycline under visible light

Renrui Sun^a, Wei Wang^a, Tianli Yang^b, Ren He^b, Jing Wang^b, Kehui Xue^b, Jun Zhou^a, Chun Long^a, Wenlei Wang^{b,*}

^aCollege of Materials Science and Engineering, Central South University of Forestry and Technology, Changsha 410004, China, emails: renrui_sun@163.com (R. Sun), weizhen.www@qq.com (W. Wang), zj2289667401@gmail.com (J. Zhou), longchunxiaokeai@163.com (C. Long)

^bCollege of Science, Central South University of Forestry and Technology, Changsha 410004, China, emails: wenlei_wang@csuft.edu.cn/wenlei_wang@hotmail.com (W. Wang), tianliyangyt1@163.com (T. Yang), heren2017@163.com (R. He), katherine95730@163.com (J. Wang), KehuiXue@163.com (K. Xue)

Received 8 November 2019; Accepted 12 May 2020

ABSTRACT

In this work, $ZrW_2O_8/CdWO_4$ nanotubes were synthesized by hydrothermal method. Electron beam irradiation was used as a means to artificially etch the interface defects and realize the reverse growth of $Zr_{1-0.5x}Cd_xW_2O_8$ at the interface of $ZrW_2O_8/CdWO_4$ nanotube. The micro-morphology and the crystal lattice of the nanotubes have changed obviously after electron beam irradiation. The XPS results for the Zr, Cd, W, and O elements confirmed the transformation of $ZrW_2O_8/CdWO_4$ to substitution solid solution of $Zr_{1-0.5x}Cd_xW_2O_8$. Fifty milliliters of 20 mg/L tetracycline could be completely degraded within 75 min by only 10 mg of ZCW-210 photocatalyst. Through fitting the kinetic experiment data, the k value of ZCW-210 could reach 0.0447 min^{-1} . Obviously, the photocatalytic performance of $ZrW_2O_8/CdWO_4$ decorated with $Zr_{1-0.5x}Cd_xW_2O_8$ has been dramatically improved compared with $ZrW_2O_8/CdWO_4$. Besides, energy band gap of the photocatalyst after electron beam irradiation has decreased from 2.86 to 2.35 eV, indicating a better utilization of visible light. Based on these experimental data, electron beam irradiation could promote the formation of heterojunctions and fabricate interface defects on the material, resulting in that the recombination of electron hole pairs in the catalytic process was inhibited. The electron paramagnetic resonance results implied that h^+ , $\cdot O_2$, and $\cdot OH$ were the main active substances in the photooxidation of tetracycline by $ZrW_2O_8/CdWO_4$ decorated with $Zr_{1-0.5x}Cd_xW_2O_8$.

Keywords: $ZrW_2O_8/CdWO_4$; Electron beam irradiation; $Zr_{1-0.5x}Cd_xW_2O_8$; Interface defects; Tetracycline

1. Introduction

The overuse of antibiotics has become a serious environmental problem in recent years [1–3]. Tetracycline (TC), as a typical antibiotic, is widely used in medical field, animal breeding, and plant cultivation [4–6]. The abuse of antibiotics

leads to continuous enhancement of bacterial resistance and the reduction of human immunity [7]. The antibiotics can flow into the human body along with water circulation and food chain, causing great harm to the ecological system [8,9]. The removal of antibiotics by photocatalytic degradation could be one of the most environmentally friendly

* Corresponding author.

methods [10,11]. Zr is a kind of d^0 configuration metal that is usually used in the synthesis of semiconductor materials. Its oxide -ZrO_2 with negative conduction band (-1.0 eV) has excellent reduction capacity and can be used in catalytic hydrogen production [12,13]. WO_3 has a layered structure. Its valence band is composed of O_{2p} and W_{4f} hybrid orbitals [14,15]. ZrW_2O_8 is a mixed oxide material, which is a negative thermal expansion material [16,17]. The heterojunction materials, such as $\text{Bi}_2\text{WO}_6/\text{CdWO}_4$ [18], $\text{Bi}_2\text{O}_2\text{CO}_3/\text{CdWO}_4$ [19], and $\text{WO}_3/\text{CdWO}_4$ [20], have received a lot of attention. They can not only overcome the defects of a single species, but also show better catalytic performance [21,22].

The construction of interface defects on the material surface has become an important means of material modification [23–25]. In general, the interface defects are beneficial for improving the performance of the material [26,27]. Some investigations have proved that the nitrogen defect of C_3N_4 helps improve its performance as a battery electrode [28–30]. Electron beam irradiation can be a treatment method widely used in sewage treatment [31], food preservation [32], and functional material treatment [33]. It has been demonstrated that high-energy particle bombardment can cause interface defects on the material surface [34,35]. High-energy electron bombardment may lead local chemical reactions, change the structure of an atom, or can remove atoms in a predetermined area [36]. Electron beam irradiation has been used to synthesize the carbon nanotubes [37]. The electron beam irradiation treatment is relatively stable with respect to energy beams such as ion beams and laser beams [38–40].

In this work, electron beam irradiation was used as the method of manufacturing interface defects. The role of interface defect on the materials has been investigated by changing different irradiation doses, focusing on the microscopic morphology and catalytic capacity of the materials. Transmission electron microscopy (TEM), energy dispersive X-ray spectroscopy (EDX), X-ray diffraction (XRD), photoluminescence (PL), N_2 adsorption and desorption isotherm (Brunauer–Emmett–Teller, BET), thermogravimetric analysis (TG), contact angle measurement (CAM), electrochemical impedance spectroscopy (EIS), solid UV visible diffuse reflectance spectrum (DRS), electron spin resonance (ESR), and other characterization methods will be used to study the micro-morphology and the crystal lattice of the material.

2. Materials and methods

2.1. Chemical reagents

Zirconium (IV) chloride (ZrCl_4), cadmium chloride ($\text{CdCl}_2 \cdot 2.5\text{H}_2\text{O}$), sodium tungstate ($\text{Na}_2\text{WO}_4 \cdot 2\text{H}_2\text{O}$), hydrochloric acid (HCl), ethylenediamine ($\text{C}_2\text{H}_8\text{N}_2$), tetracycline (TC) were all bought from Sinopharm Chemical Reagent Co. Ltd., Shanghai Province, China. Deionized water (DIW) was supplied through a Milli-Q water purification system and used in all experiments.

2.2. Catalyst synthesis

In order to synthesize CdWO_4 nanorods, 1 mmol $\text{CdCl}_2 \cdot 2.5\text{H}_2\text{O}$ and 5 mmol of $\text{Na}_2\text{WO}_4 \cdot 2\text{H}_2\text{O}$ were dissolved in 20 mL deionized water. After that, 1 mL ethylenediamine was dropwise added to the above solution under continuous

stirring. Hydrochloric acid solution was used to adjust the pH of the aqueous nitrate solution to 7. The mixture was transferred to the reaction kettle with continuously stirring for further reaction. Then, the reactor was heated under 200°C for 3 h. The generated powder was separated by filtration, and washed with ethanol and de-ionized water for three times. The final product was dried at 60°C for 6 h, and was named as CW.

The $\text{ZrW}_2\text{O}_8/\text{CdWO}_4$ composite was prepared by a hydrothermal method. Firstly, 0.4 mmol ZrOCl_2 was dissolved into deionized water, and 1 mmol $\text{Na}_2\text{WO}_4 \cdot 2\text{H}_2\text{O}$ was dissolved into 1 mol/L hydrochloric acid. And then, the above two solutions were slowly mixed to maintain the pH of the mixture at 1.2. After that, 1 mmol of the as-prepared CdWO_4 was added to the above solution. The mixture was transferred to a reactor and kept at 160°C for 24 h. The precipitate was washed three times with deionized water, and was dried in an oven at 40°C for 24 h. Finally, the sample was transferred to a combustion boat, and was heated in a tube furnace at 600°C for 6 h. The $\text{ZrW}_2\text{O}_8/\text{CdWO}_4$ was got, and was named as ZCW. Pure ZrW_2O_8 was referred to be as ZW in subsequent analyses.

2.3. Defects treatment

After the samples were uniformly dispersed on the glass sheet, the materials were irradiated by electron beam irradiation. The time required for each cycle of irradiation was 7.5 min, and the irradiation intensity provided by one cycle was 30 KGy. Therefore, 90, 210, and 480 KGy were selected as the experimental exploration dose, and the samples treated with corresponding irradiation dose were named as ZCW-90, ZCW-210, and ZCW-480, respectively.

2.4. Photocatalytic experiment

The effect of interface defects on catalytic performance of the material will be directly reflected by the degradation efficiency of TC. In these experiments, the concentration of TC was 20 mg/L, the mass of the photocatalyst used was 10 mg, and the volume of the waste liquid was 50 mL. In elimination of the interference of adsorption on the experimental results, the photocatalyst and waste liquid will be stirred continuously under dark conditions for 45 min to achieve the adsorption equilibrium. The concentration of waste liquid was measured by liquid chromatography.

2.5. Characterization

For better understanding the properties of the obtained materials, TEM with an operating voltage of 200 kV (Tecnai G2 F20 S-TWIN TMP, USA), XRD equipped with Cu $K\alpha$ radiation and the scat speed of $0.2^\circ/\text{min}$ (X' Pert PRO, Holland), BET (TriStar II 3flex, USA), TG (USA, TA Q500), XPS operated at 10 mA and 15 kV (4.5×10^{-9} Torr pressure) (EscaLab Xi+, USA), DRS with BaSO_4 as reference (Lambda 750 S, USA), EIS (PP211 and CHI1030B, Germany), PL with the scanning speed of 1,200 nm/min and the emission slit width of 5.0 nm (F-7000, Hitachi, Japan), ESR (Bruker a300, Germany) and other characterization methods have been used in this work.

3. Results and discussion

3.1. Effects of interface defects on the morphology of materials

An effect simulation diagram has been constructed to simulate the load of ZrW_2O_8 on $CdWO_4$ nanorods and the treatment of materials by electron beam irradiation, as shown in Fig. 1. The obtained $ZrW_2O_8/CdWO_4$ presented the morphology of rod-like structure with uniform particle size with length of 100 nm and diameter of 25 nm. $CdWO_4$ has occurred as the matrix, and ZrW_2O_8 has been uniformly attached on the interface of $CdWO_4$. Electron beam irradiation has reconstructed the interface between different materials.

EDX spectrum (Fig. 2a) confirmed the elements composition of the $ZrW_2O_8/CdWO_4$ decorated with $Zr_{1-0.5x}Cd_xW_2O_8$. The existence of strong signal peaks representing Zr, Cd, W, and O in samples proved the successful synthesis of $ZrW_2O_8/CdWO_4$ heterojunction. The element composition analysis of the material was based on copper mesh, resulting in that there was a strong Cu peak in the EDX spectrum. XRD (about 20 mg sample) spectrum was used to evaluate the crystal structure of the photocatalyst, as shown in Fig. 2b. These data were consistent with the standard cards (JCPDS No. 13-0514, JCPDS No. 50-1868). The photocatalysts after electron beam irradiation had different signal peaks of 24.3° , 25.6° , and 34.2° that were different from the pure $CdWO_4$ and ZrW_2O_8 . These peaks might be corresponded to the formation of $Zr_{1-0.5x}Cd_xW_2O_8$ solid solution. It can be found that the sample corresponding to the irradiation dose of 210 KGy had the sharpest peak, indicating that the best effect of interface reconstruction can be achieved at this dose. The signal peaks appeared at 34.6° and 47.9° could be corresponded to Zr^0 (JCPDS No. 65-3366) with the irradiation dose increasing to 480 KGy. In this case, some Zr^0 quantum dots had a large delocalization, resulting in leaving the original crystal configuration and forming a single atom or substance. Subsequently, these quantum dots can converge to produce Zr clusters.

HRTEM was used to clearly observe the specific impact of electron beam irradiation on the material surface. Figs. 3a–d corresponded to ZCW, ZCW-90, ZCW-210, and ZCW-480, respectively. With the increasing of irradiation dose, the crystal surface of the material changed from ordered arrangement to disorder arrangement. At the dose of 210 KGy, the migration and dislocation of atomic arrangement began to occur, and the original regular lattice arrangement of the material gradually disappeared. At the dose of 480 KGy, the surface structure of the material had serious defects and even eutectic phenomenon. At larger doses, some bright spots were found on the material's surface. It was possible that the high electronegative energy helped liberate the metal atoms bound by chemical bonds. Thus, a single Zr atom may be produced. This treatment strategy provides a new idea for the synthesis of monatomic catalysts or quantum dot catalysts [41].

3.2. Effects of interface defects on specific properties of materials

Surface chemical states of ZCW and ZCW-210 have been studied by the means of XPS analysis with 20–30 mg sample. As shown in Fig. 4a, two main peaks of Zr 3d were 182.5 and 184.9 eV, which could be corresponded to Zr $3d_{5/2}$ and Zr $3d_{3/2}$ in consistent with Zr–O bond of $ZrW_2O_8/CdWO_4$ crystal structure. The decrease of specific binding energy was attributed to the change of the stable octahedron structure irradiated by electron beam. It can be seen that the corresponding signal peaks of Cd in the material without electron beam irradiation were 404.9 and 411.6 eV, while the specific binding energy of Cd after treatment increased to 405.3 and 412.2 eV, respectively (Fig. 4b). Combined with the XRD data, it can be inferred that, the interfacial defects caused by electron beam irradiation led to the interfacial reconstruction of the heterogeneous joint surface of the material, resulting in the formation of $Zr_{1-0.5x}Cd_xW_2O_8$ solid solution. Compared with the Cd–O bond, the newly formed Cd–O–Zr bond had a stronger specific binding energy.



Fig. 1. Schematic diagram of the synthesis process and TEM diagram of the final product.

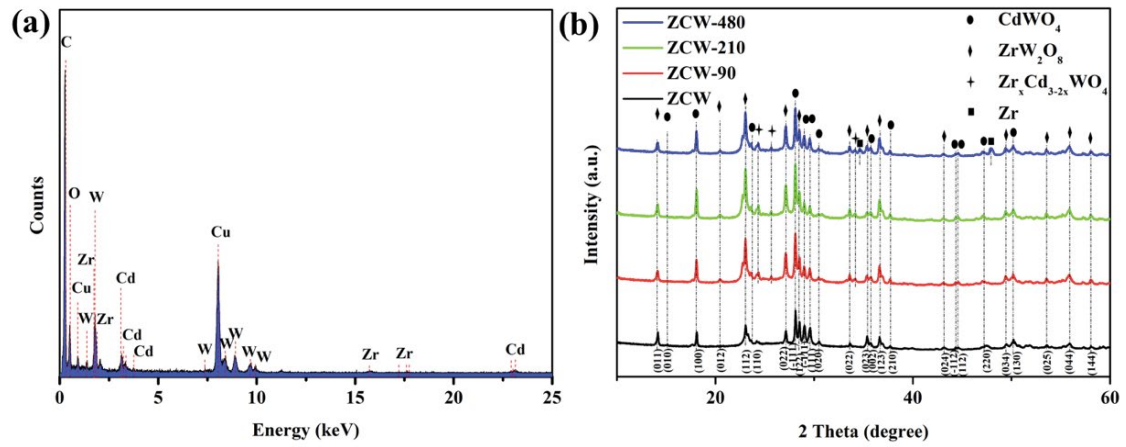


Fig. 2. $\text{ZrW}_2\text{O}_8/\text{CdWO}_4$ EDX spectrum data (a) and XRD pattern of the samples (b).

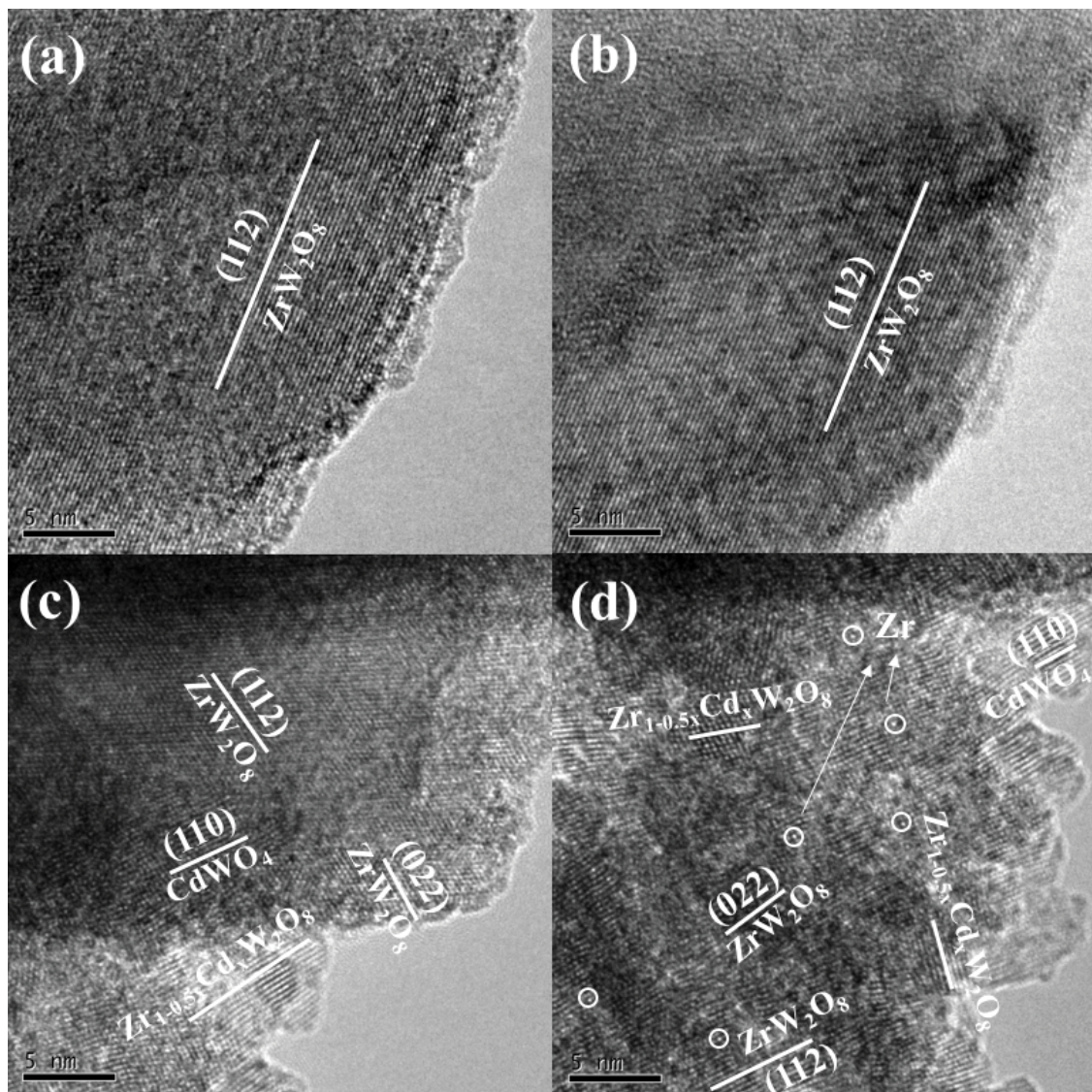


Fig. 3. TEM of ZCW (a), ZCW-90 (b), ZCW-210 (c), and ZCW-480 (d). The number represents the irradiation dose.

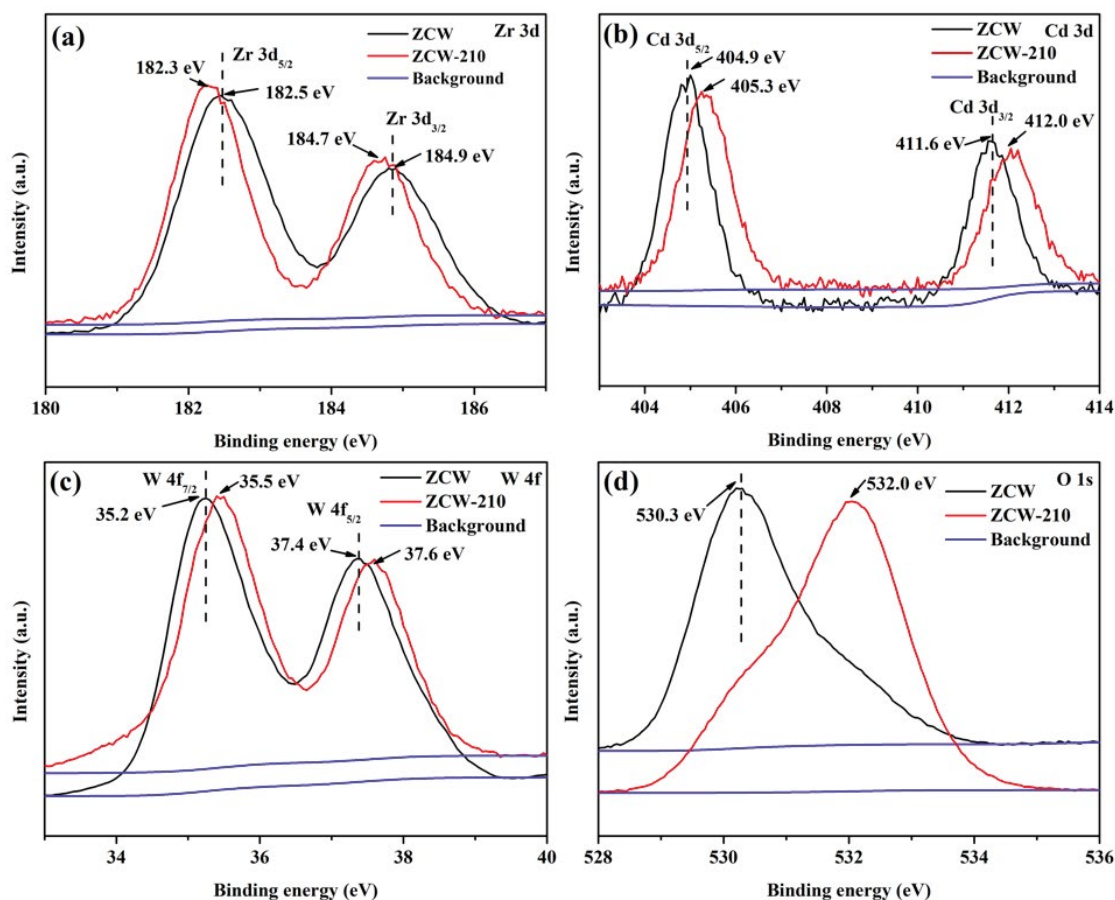


Fig. 4. XPS results of ZCW and ZCW-210: Zr 3d (a), Cd 3d (b), W 4f (c), and O 1s (d).

Also, the specific binding energies of the two signal peaks corresponding to the W_{4f} orbital have increased to a certain extent. This inference could also be supported by the significant increase in the orbital binding energy from 530.3 to 532.0 eV in Fig. 4d. The lattice hybridization caused by interfacial defect promoted the formation of solid solution. This might be one of the reasons for the increase of the binding energy of O 1s.

What's more, in order to investigate the influence of electron beam irradiation on the specific surface area of materials, BET (more than 500 mg) experiment has been conducted with degassing time of 10 h and degassing temperature of 150°C. The results are shown in Fig. 5, where Figs. 5a–d represent ZCW, ZCW-90, ZCW-210, and ZCW-480, respectively. The specific area of the material slightly increased with the increase of irradiation dose. The pore size distribution data of each material were also analyzed. It was found that the increase of the maximum pore size in the material was positively correlated with the increase of the electron beam irradiation dose. It was noteworthy that there was a different trend, that was, a large number of pore structures with average pore diameter of about 7–8 nm appeared when the irradiation dose increased to 210 and 480 KGy. The interface defect was beneficial to the increase of the specific surface area. Moreover, interface defects caused by larger dose of electron beam irradiation could

etch tiny holes on the surface of materials. It was conducive to the adsorption capacity of materials and provided more active sites when catalytic reactions occurred.

Thermal stability (20 mg sample) was one of indexes to measure the stability of the photocatalysts. The atmosphere of the test gas is nitrogen, and the heating rate of the test was 10°C/min. The detection range was from 25°C to 1,000°C. The relevant results are shown in Fig. 6a. It can be seen that the material had a rapid weightlessness with increasing temperature before 100°C, which might be caused by the partial removal of adsorbed water molecules. The thermal weightlessness at the 100°C–400°C stage might be caused by a small amount of $ZrW_2O_7(OH)_2(H_2O)_2$ produced in the material synthesis process. At this stage, the material lost its crystal water and disintegrated into ZrW_2O_8 . Thereafter, the mass of the material changed slightly, which was because the lattice arrangement of the material gradually transformed from orthogonal to tetragonal. In tetragonal system, the bonding force between ZrO_6 octahedron and WO_4 tetrahedron of the material was small, and the coupling rotation between the two polyhedrons was easy to occur. Another severe weight loss at 850°C was caused by the decomposition of ZrW_2O_8 into ZrO_2 and WO_3 , and WO_3 significantly sublimated at this temperature. In general, there was less crystallization water in the materials after electron beam irradiation, and the interface defects generated by electron

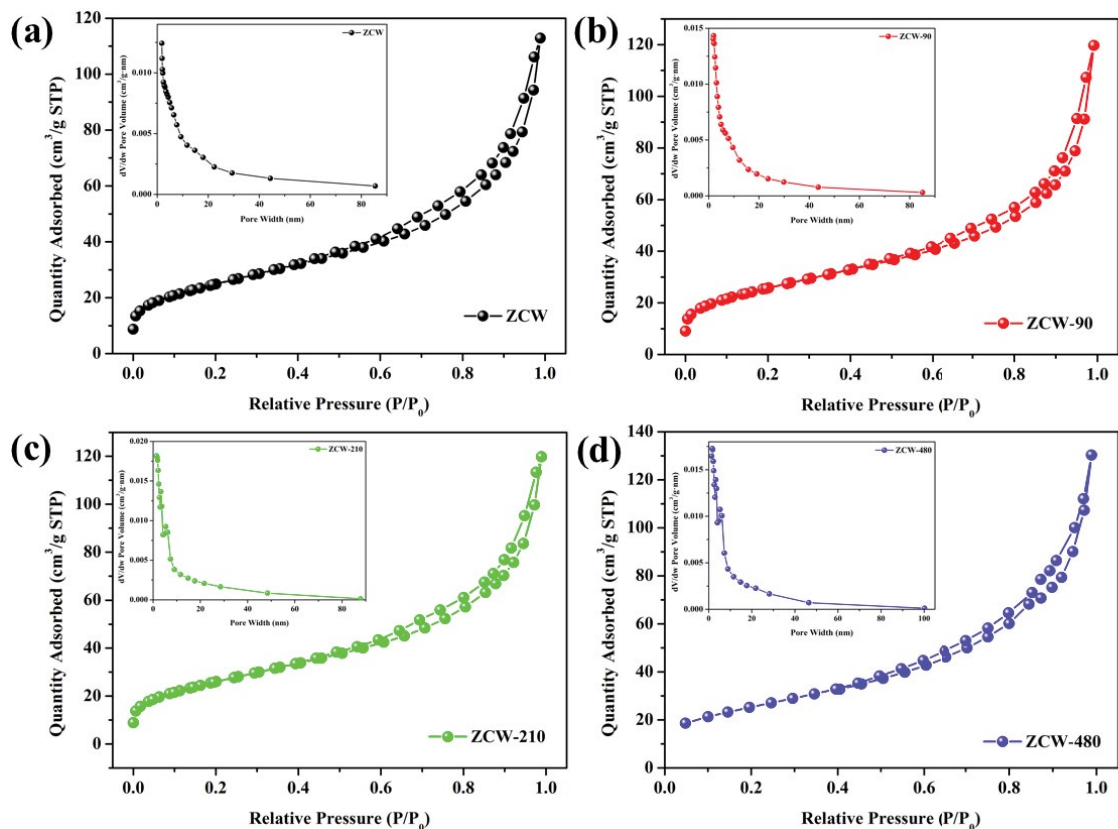


Fig. 5. Nitrogen adsorption and desorption isotherm of the as-prepared ZCW (a), ZCW-90 (b), ZCW-210 (c), and ZCW-480 (d) nano-meter heterogeneous materials, and corresponding pore size distribution data.

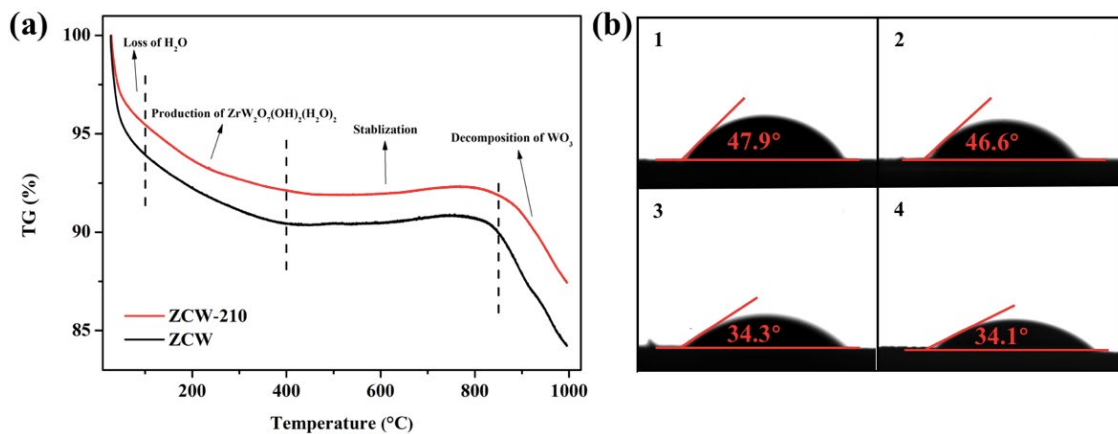


Fig. 6. Thermogravimetric analysis of materials (a), contact angle image of sample ZCW (b1), ZCW-90 (b2), ZCW-210 (b3), and ZCW-480 (b4).

beam irradiation could not possess great impact on the thermal stability of the material. The influence of electron beam irradiation dose on the hydrophilic and hydrophobic properties of the as-prepared photocatalyst was verified by using contact angle tester, as shown in Fig. 6b. The contact angles of the droplet experiments of ZCW, ZCW-90, ZCW-210, and ZCW-480 were 47.9°, 46.6°, 34.3°, and 34.1°, respectively, indicating that the surface roughness of the material gradually increased with the increase of the radiation dose.

3.3. Photocatalytic properties of ZrW₂O₇/CdWO₄ decorated with Zr_{1-0.5x}Cd_xW₂O₈

Specific photocatalytic experimental results are shown in Fig. 7a. The higher the irradiation dose was, the better the adsorption capacity of TC was carried out. The interface defect was beneficial to the improvement of specific surface area and the enhancement of adsorption capacity. Comparing with ZW, ZCW with interface defects had better

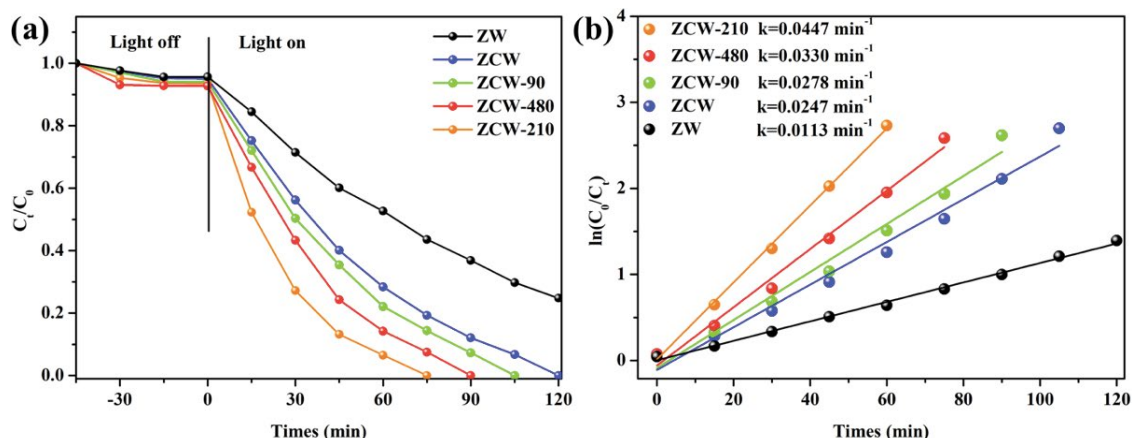


Fig. 7. Photocatalytic degradation of TC (a) and kinetic plot of different samples (b).

catalytic degradation ability to degrade TC. However, the interface defects produced by excessive irradiation dose were not conducive to the improvement of catalytic properties. Fig. 7b is the first-order kinetic equation fitting for degradation rate, and the first-order reaction equation was $\ln(C_t/C_0) = kt$. The larger k value represented the faster degradation rate. The degradation capacity of $\text{ZrW}_2\text{O}_8/\text{CdWO}_4$ heterojunction was twice that of ZrW_2O_8 , and the degradation capacity of the obtained photocatalysts with electron beam irradiation dose of 210 KGy was nearly twice that of untreated materials. Comparing with CdS/titano-oxo-cluster nanocomposites which required complex synthesis methods [42], the materials synthesized in this work can also achieve 70% of its high catalytic activity.

Exploring the cyclic stability of catalytic materials with interface defects is quite important. The results are shown in Table 1. The volume and concentration of waste liquids in the cycle experiment stage were consistent with the first experiment, and the catalyst was reused after centrifugation, washing, and drying. The reference criterion for the digital percentage was the first catalytic degradation efficiency. Obviously, ZrW_2O_8 showed poor cycle stability. Besides, the photocatalyst with the radiation dose of 90 and 210 KGy did not affect the stability of the material, and its catalytic stability was similar to that of ZCW. However, when the irradiation dose increased to 480 KGy, the cyclic stability of the material got a decline. The electron beam irradiation caused the material structure to be loose and easy to fall off or disintegrate.

Band gap was an important index of the properties for semiconductor materials. The ultraviolet diffuse reflection

spectrum of the material at 200–800 nm was analyzed. As shown in Fig. 8a, the optical response of the material occurred within the absorption sideband range of 300–450 nm. Fig. 8b is the material band gap data which is obtained according to Tauc plot equation. It can be clearly seen that the material treated by electron beam irradiation had a smaller band gap, and the material treated by 210 KGy irradiation dose had a significant reduction from 2.84 to 2.35 eV. Electron hole pairs were more easily used for catalytic degradation of materials after separation due to the shortened transport path of photogenic carriers, and the utilization rate of photocatalytic materials to photogenerated carriers was an index to measure their catalytic ability. On this premise, the photoluminescence spectrum had been measured. The result is shown in Fig. 8c. The lower the intensity signal is, the higher the utilization of photogenerated carriers is. It was obviously that the composition of ZrW_2O_8 and CdWO_4 could effectively improve the utilization of photogenerated carriers than that of pure ZrW_2O_8 . This meant that the recombination of electron-hole pairs was inhibited owing to the participation of interface defect in the catalytic process. When the irradiation dose increased to 480 KGy, the PL strength of the material showed an increasing trend, indicating that excessive interfacial defect inhibited the utilization of photonic carriers. Interfacial defects might also affect the photochemical properties of the materials, so we characterized the transient photocurrent response and electrochemical impedance of the products. As can be seen from the electrochemical impedance diagram in Fig. 8d, the Nyquist plot of ZCW-210 composite material was the

Table 1
Catalytic capacity data of different samples (Pure ZrW_2O_8 , ZCW, ZCW-90, ZCW-210, and ZCW-480) after different cycles

Cycle times samples	1	2	3	4	5
ZW	97.31%	95.12%	92.98%	91.06%	89.17%
ZCW	99.13%	98.32%	96.69%	94.27%	93.44%
ZCW-90	99.21%	98.26%	96.38%	95.00%	93.78%
ZCW-210	98.92%	97.94%	96.47%	93.88%	93.45%
ZCW-480	98.26%	96.33%	95.10%	93.41%	90.52%

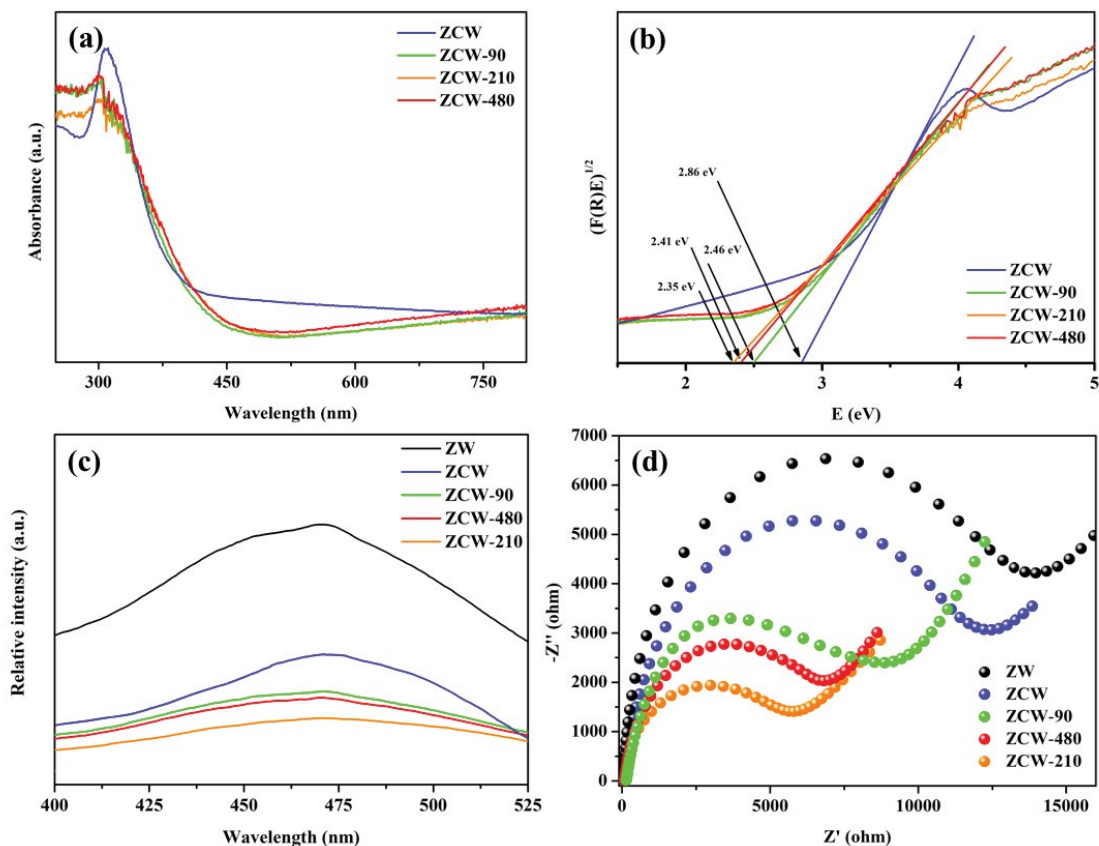


Fig. 8. DRS dates of the samples (a) and determined by the Tauc plot (b), PL spectra of ZW, ZCW, ZCW-90, ZCW-210, and ZCW-480 (c), and electrochemical impedance spectroscopy (EIS) analysis of ZW, ZCW, ZCW-90, ZCW-210, and ZCW-480 (d).

smallest compared with $ZrW_2O_8/CdWO_4$ and other dose-treated samples. The above test results indicated that the reconstruction of material heterojunction caused by interface defect could improve the efficiency of charge transport and reduce the recombination rate of carriers.

3.4. Study on degradation of tetracycline

Finding the catalytic active groups involved in the reaction process is important. Before the photocatalytic experiment, triethanolamine (TEOA), 1,4-benzoquinone (BQ), and isopropanol (IPA) had been added into the reaction system as the scavenger for hole (h^+), superoxide radical ($\cdot O_2^-$) and hydroxyl radical ($\cdot OH$), respectively [43,44]. The other conditions remained unchanged, and the concentration of waste liquid obtained after the same time will be measured. The additional scavenger of TEOA and IPA reduced the degradation efficiency to 37.84% and 32.16%, respectively. This proved that both h^+ and $\cdot OH$ played key roles in catalytic reactions. The addition of BQ dramatically reduced the degradation efficiency of materials to 27.36%, which proved that $\cdot O_2^-$ also played a crucial role in the oxidation process of TC. In order to further confirm this point, the experiment of oxygen removal was also carried out, that is, nitrogen was injected into the solution. The results showed that the entry of N_2 greatly hindered the removal of TC, and the removal rate of TC decreased

from 96.21% to 57.67%, this proved that the dissolved oxygen in water can combine with photogenic electrons to produce $\cdot O_2^-$ free radical and then degrade TC [45]. The high content of dissolved oxygen in water was conducive to the catalytic degradation of materials. The above experimental results showed that the three catalytic active groups were involved in the catalytic reaction, so we carried out a further analysis of them. h^+ spin capture occurred in the 1% phosphate buffer solution containing 2,2,6,6-tetramethylpiperidine (TEMPO) spin capture reagent. The capture of $DMPO\cdot O_2^-$ occurred in methanol solution, while the capture of $DMPO\cdot OH$ occurred in aqueous solution. Their ESR data are shown in Figs. 9b–d, respectively. It was noteworthy that holes had strong model peaks under dark conditions, but when the illumination time was 5 min, its signal peak decreased rapidly. This indicated that the holes (h^+) were effectively utilized in the catalytic process, which suggested that the holes were the important catalytic active group in the catalytic process. For $DMPO\cdot O_2^-$, there was no obvious characteristic peak in dark condition. After 5 min of light, several strong characteristic peaks appeared, which validated that $\cdot O_2^-$ was largely involved in catalytic reactions. Besides, the results of $DMPO\cdot OH$ were similar to the $DMPO\cdot O_2^-$. There was no clear signal in the dark, but a high signal peak appeared after 5 min of light. The three sets of data indicated that all the three active substances participated in the photocatalytic reaction process of the

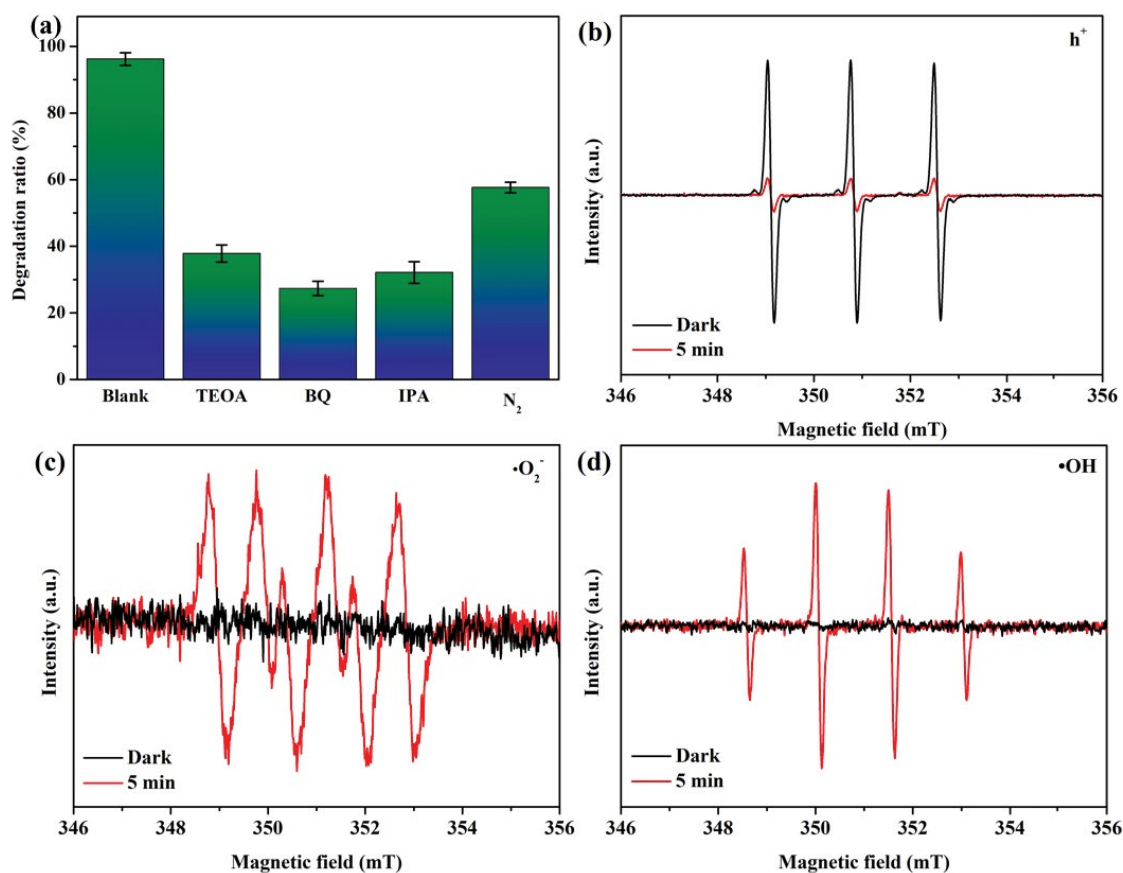
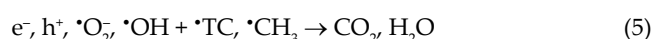
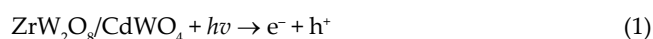


Fig. 9. Comparison of effects of different scavengers on catalytic degradation of materials under illumination (a) and ESR spectra of the ZCW-210 catalytic active groups at darkness and illumination for 5 min: TEMPO-h⁺ (b), DMPO-[•]O₂⁻ (c), and DMPO-[•]OH (d).

material and played a role in the degradation of tetracycline. Combined with other characterization results, the imperfection of the interface caused by electron beam irradiation was beneficial to the production of catalytic active substances at the catalytic interface. Due to the formation of solid solution heterojunctions, the conduction of active electrons was more efficient, and the recombination of electron hole pair was strongly inhibited [46]. Herein, through comparison of research by Chen et al. [47] the materials synthesized in this experiment have significantly improved the catalytic activity of h⁺ and [•]OH in the catalytic process of tetracycline. This made the experimental material at the same catalyst dosage and the same tetracycline concentration, was more than twice its catalytic capacity.

Based on the analysis of known data and relevant literatures, we speculated that ZrW₂O₈/CdWO₄ heterojunction materials generated electrons and holes in the light excitation (e.1). Among them, h⁺ took the lead in the degradation of tetracycline, and a demethylation process occurred in tetracycline (e.2) [42]. As the catalytic process progresses, the electrons combined with dissolved oxygen in the water to form [•]O₂⁻ (e.3). Meanwhile, h⁺ reacted with water at the catalytic interface of the material to form hydroxyl radical ([•]OH) and free H⁺ (e.4). Subsequently, the generated h⁺, [•]O₂⁻, [•]OH gradually degraded [•]TC, [•]CH₃ into small molecules of CO₂ and H₂O in the catalytic system (e.5). Since the diversity

of active substances in catalytic materials, and the generated [•]TC was easy to combine with [•]O₂⁻ for oxidation reaction. These may be the reason why the material can degrade tetracycline efficiently [48,49]. The simulation of the entire catalytic process is shown in Fig. 10.



4. Conclusion

In order to find a kind of material with superior photocatalytic activity for degradation of tetracycline under visible light, several electron beam irradiation doses were selected to control the interface defects onto CdWO₄/ZrW₂O₈, and realize the reverse growth of Zr_{1-0.5x}Cd_xW₂O₈ at the interface of ZrW₂O₈/CdWO₄ nanotube. Intuitively, the micro-morphology of the material has changed, and the lattice of the material tended to disorder due to a large

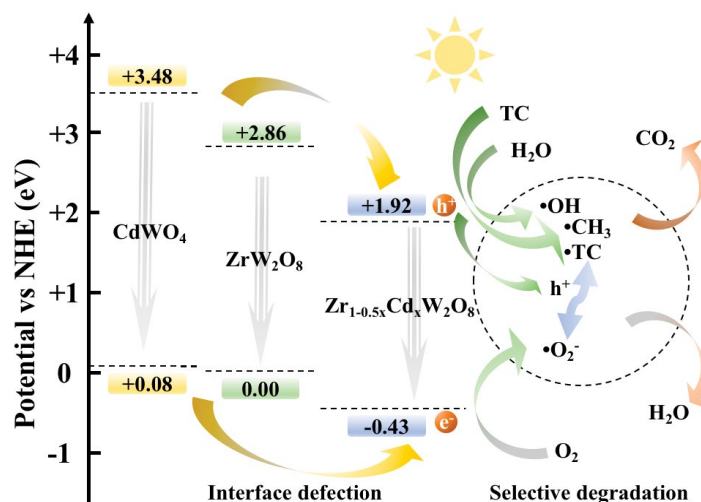


Fig. 10. Diagram of the material degradation process.

degree of interfacial defect. Changes in XPS bandgaps of Zr, Cd, W, and O indicated the transformation of ZrW₂O₈/CdWO₄ to substitution solid solution of Zr_{1-0.5x}Cd_xW₂O₈. The catalytic performance for ZrW₂O₈/CdWO₄ decorated with Zr_{1-0.5x}Cd_xW₂O₈ has been dramatically improved compared with ZrW₂O₈ alone. Degradation time of a certain amount of tetracycline by the as-prepared materials treated with 210 KGy irradiation dose was reduced from 120 to 75 min. Energy band gap of the photocatalyst decreased from 2.86 to 2.35 eV, which meant a better utilization of visible light. Electron beam irradiation promoted the formation of heterojunctions and fabricated interface defects, resulting in that the recombination of electron hole pairs in the catalytic process was inhibited. From the results of photocatalysis, the chaotic lattice might cause excessive conduction “paths” and affect the conduction of electrons. Due to the participation of h⁺, •O₂⁻, •OH, tetracycline was high-selectivity degraded by ZrW₂O₈/CdWO₄ decorated with Zr_{1-0.5x}Cd_xW₂O₈.

Acknowledgments

The authors gratefully acknowledge the financial support of the National Natural Science Foundation of China (Grant No: 41977129, 21607176, and 31670563), Changsha outstanding innovative youth training program (Grant No. kq1802011), the Natural Science Foundation of Hunan Province, China (Grant No. 2017JJ3516), the Research Foundation of Education Bureau of Hunan Province, China (Grant No. 16B274), and the Innovation Fund for Post-graduates of Central South University of Forestry and Technology (Grant No. CX20192023). The authors also thank the reviewers for their constructive comments and suggestions.

References

- [1] A.K. Sarmah, M.T. Meyer, A.B.A. Boxall, A global perspective on the use, sales, exposure pathways, occurrence, fate and effects of veterinary antibiotics (VAs) in the environment, *Chemosphere*, 65 (2006) 725–759.
- [2] B. Wang, X.L. Lv, D.W. Feng, L.H. Xie, J. Zhang, M. Li, Y.B. Xie, J.R. Li, H.C. Zhou, Highly stable Zr(IV)-based metal-organic frameworks for the detection and removal of antibiotics and organic explosives in water, *J. Am. Chem. Soc.*, 138 (2016) 6204–6216.
- [3] S. Rodriguez-Mozaz, S. Chamorro, E. Marti, B. Huerta, M. Gros, A. Sanchez-Melsio, C.M. Borrego, D. Barcelo, Occurrence of antibiotics and antibiotic resistance genes in hospital and urban wastewaters and their impact on the receiving river, *Water Res.*, 69 (2015) 234–242.
- [4] I. Chopra, M. Roberts, Tetracycline antibiotics: mode of action, applications, molecular biology, and epidemiology of bacterial resistance, *Microbiol. Mol. Biol. Rev.*, 65 (2001) 232–260.
- [5] N. Li, L. Zhou, X.Y. Jin, G. Owens, Z.L. Chen, Simultaneous removal of tetracycline and oxytetracycline antibiotics from wastewater using a ZIF-8 metal organic-framework, *J. Hazard. Mater.*, 366 (2019) 563–572.
- [6] M.A. Kohanski, D.J. Dwyer, B. Hayete, C.A. Lawrence, J.J. Collins, A common mechanism of cellular death induced by bactericidal antibiotics, *Cell*, 130 (2007) 797–810.
- [7] M.R. Gillings, Evolutionary consequences of antibiotic use for the resistome, mobilome, and microbial pangenome, *Front. Microbiol.*, 4 (2013) 1–10.
- [8] N.L. Millar, S. Siebert, I.B. McInnes, Europe rules on antibiotic harm, *Nature*, 566 (2019) 326–326.
- [9] D.I. Andersson, D. Hughes, Antibiotic resistance and its cost: is it possible to reverse resistance, *Nat. Rev. Microbiol.*, 8 (2010) 260–271.
- [10] S.K. Ray, D. Dhakal, G. Gyawali, B. Joshi, A.R. Koirala, S.W. Lee, Transformation of tetracycline in water during degradation by visible light driven Ag nanoparticles decorated alpha-NiMoO₄ nanorods: mechanism and pathways, *Chem. Eng. J.*, 373 (2019) 259–274.
- [11] S. Kment, F. Riboni, S. Pausova, L. Wang, L.Y. Wang, H. Han, Z. Hubicka, J. Krysa, P. Schmuki, R. Zboril, Photoanodes based on TiO₂ and alpha-Fe₂O₃ for solar water splitting - superior role of 1D nanoarchitectures and of combined heterostructures, *Chem. Soc. Rev.*, 46 (2017) 3716–3769.
- [12] H.R. Pouretedal, Z. Tofangsazi, M.H. Keshavarz, Photocatalytic activity of mixture of ZrO₂/SnO₂, ZrO₂/CeO₂ and SnO₂/CeO₂ nanoparticles, *J. Alloys Compd.*, 513 (2012) 359–364.
- [13] R. Sasikala, A.R. Shirole, S.R. Bharadwaj, Enhanced photocatalytic hydrogen generation over ZrO₂-TiO₂-CdS hybrid structure, *J. Colloid Interface Sci.*, 409 (2013) 135–140.
- [14] B. Song, T.T. Wang, H.G. Sun, Q. Shao, J.K. Zhao, K.K. Song, L.H. Hao, L. Wang, Z.H. Guo, Two-step hydrothermally synthesized carbon nanodots/WO₃ photocatalysts with enhanced photocatalytic performance, *Dalton Trans.*, 46 (2017) 15769–15777.
- [15] S.G. Kumar, K.S.R.K. Rao, Comparison of modification strategies towards enhanced charge carrier separation and photocatalytic

- degradation activity of metal oxide semiconductors (TiO₂, WO₃ and ZnO), *Appl. Surf. Sci.*, 391 (2017) 124–148.
- [16] L. Jiang, Q.Z. Wang, C.L. Li, J.A. Yuan, W.F. Shangguan, ZrW₂O₈ photocatalyst and its visible-light sensitization via sulfur anion doping for water splitting, *Int. J. Hydrogen Energy*, 25 (2010) 7043–7050.
- [17] Y.A. Sethi, R.P. Panmand, S.R. Kadam, A.K. Kulkarni, S.K. Apte, S.D. Nails, N. Munirathnam, M.V. Kulkarni, B.B. Kale, Nanostructured CdS sensitized CdWO₄ nanorods for hydrogen generation from hydrogen sulfide and dye degradation under sunlight, *J. Colloid Interface Sci.*, 487 (2017) 504–512.
- [18] P. Chen, L. Chen, Y. Zeng, F. Ding, X. Jiang, N. Liu, C.T. Au, S.F. Yin, Three-dimension hierarchical heterostructure of CdWO₄ microrods decorated with Bi₂WO₆ nanoplates for high-selectivity photocatalytic benzene hydroxylation to phenol, *Appl. Catal., B*, 234 (2018) 311–317.
- [19] C.M. Yang, G.M. Gao, J.J. Zhang, R.P. Liu, R.C. Fan, M. Zhao, Y.W. Wang, S.C. Gan, Surface oxygen vacancy induced solar light activity enhancement of a CdWO₄/Bi₂O₂CO₃ core-shell heterostructure photocatalyst, *Phys. Chem. Chem. Phys.*, 19 (2017) 14431–14441.
- [20] I. Aslam, C.B. Cao, M. Tanveer, M.H. Farooq, W.S. Khan, M. Tahir, F. Idrees, S. Khalid, A novel Z-scheme WO₃/CdWO₄ photocatalyst with enhanced visible-light photocatalytic activity for the degradation of organic pollutants, *RSC Adv.*, 5 (2015) 6019–6026.
- [21] H.W. Huang, X. Han, X.W. Li, S.C. Wang, P.K. Chu, Y.H. Zhang, Fabrication of multiple heterojunctions with tunable visible-light-active photocatalytic reactivity in BiOBr–BiOI full-range composites based on microstructure modulation and band structures, *ACS Appl. Mater. Interfaces*, 7 (2015) 482–492.
- [22] Y.L. Tian, B.B. Chang, J.L. Lu, J. Fu, F.N. Xi, X.P. Dong, Hydrothermal synthesis of graphitic carbon nitride–Bi₂WO₆ heterojunctions with enhanced visible light photocatalytic activities, *ACS Appl. Mater. Interfaces*, 5 (2013) 7079–7085.
- [23] J.F. Banfield, S.A. Welch, H. Zhang, T.T. Ebert, R.L. Penn, Aggregation-based crystal growth and microstructure development in natural iron oxyhydroxide biomineralization products, *Science*, 289 (2000) 751–754.
- [24] K. Szot, W. Speier, G. Bihlmayer, R. Waser, Switching the electrical resistance of individual dislocations in single-crystalline SrTiO₃, *Nat. Mater.*, 5 (2006) 312–320.
- [25] C. Tang, H.F. Wang, X. Chen, B.Q. Li, T.Z. Hou, B.S. Zhang, Q. Zhang, M.M. Titirici, F. Wei, Topological defects in metal-free nanocarbon for oxygen electrocatalysis, *Adv. Mater.*, 28 (2016) 6845–6851.
- [26] Y.A. Vlasov, X.Z. Bo, J.C. Sturm, D.J. Norris, On-chip natural assembly of silicon photonic bandgap crystals, *Nature*, 414 (2001) 289–293.
- [27] F. Banhart, J. Kotakoski, A.V. Krasheninnikov, Structural defects in graphene, *ACS Nano*, 5 (2011) 26–41.
- [28] J.J. Chen, Z.Y. Mao, L.X. Zhang, D.J. Wang, R. Xu, L.J. Bie, B.D. Fahlman, Nitrogen-deficient graphitic carbon nitride with enhanced performance for lithium ion battery anodes, *ACS Nano*, 11 (2017) 12650–12657.
- [29] G.C. Shearer, S. Chavan, S. Bordiga, S. Svelle, U. Olsbye, K.P. Lillerud, Defect engineering: tuning the porosity and composition of the metal-organic framework UiO-66 via modulated synthesis, *Chem. Mater.*, 28 (2016) 3749–3761.
- [30] Y.J. Liu, S.J. Li, H.L. Wang, W.T. Hou, Y.L. Hao, R. Yang, T.B. Sercombe, L.C. Zhang, Microstructure, defects and mechanical behavior of beta-type titanium porous structures manufactured by electron beam melting and selective laser melting, *Acta Mater.*, 113 (2016) 56–57.
- [31] J. Paul, K.P. Rawat, K.S.S. Sarma, S. Sabharwal, Decoloration and degradation of reactive red-120 dye by electron beam irradiation in aqueous solution, *Appl. Radiat. Isot.*, 69 (2011) 982–987.
- [32] A. Fernandes, J.C.M. Barreira, A.L. Antonio, A. Rafalski, M.B.P.P. Oliveira, A. Martins, I.C.F.R. Ferreira, How does electron beam irradiation dose affect the chemical and antioxidant profiles of wild dried Amanita mushrooms? *Food Chem.*, 182 (2015) 309–315.
- [33] Q.M. Su, G.H. Du, B.S. Xu, *In situ* growth of In₂O₃ nanocrystals by electron irradiation in transmission electron microscope, *Mater. Lett.*, 120 (2014) 208–211.
- [34] Y.Q. Wang, Y. Feng, F. Mo, G. Qian, Y.M. Chen, D.B. Yu, Y. Wang, X.B. Zhang, Influence of irradiation upon few-layered graphene using electron-beams and gamma-rays, *Appl. Phys. Lett.*, 105 (2014) 023102.
- [35] Y.J. Kwon, H.Y. Cho, H.G. Na, B.C. Lee, S.S. Kim, H.W. Kim, Improvement of gas sensing behavior in reduced graphene oxides by electron-beam irradiation, *Sens. Actuators, B*, 203 (2014) 143–149.
- [36] R. Hristu, S.G. Stanciu, D.E. Tranca, G.A. Stanciu, Electron beam influence on the carbon contamination of electron irradiated hydroxyapatite thin films, *Appl. Surf. Sci.*, 346 (2015) 342–347.
- [37] A.V. Krasheninnikov, F. Banhart, Engineering of nanostructured carbon materials with electron or ion beams, *Nat. Mater.*, 6 (2007) 723–733.
- [38] D.K. Wang, B.K. Chen, Z.P. Wei, X. Fang, J.L. Tang, D. Fang, A. Aierken, X.H. Wang, H. Maliya, Q. Guo, Electron irradiation-induced defects and photoelectric properties of Te-doped GaSb, *J. Phys. Chem. Solids*, 132 (2019) 26–30.
- [39] D. Teweldebrhan, A.A. Balandin, Modification of graphene properties due to electron-beam irradiation, *Appl. Phys. Lett.*, 94 (2009) 013101.
- [40] J.S. Bak, J.K. Ko, Y.H. Han, B.C. Lee, I.G. Choi, K.H. Kim, Improved enzymatic hydrolysis yield of rice straw using electron beam irradiation pretreatment, *Bioresour. Technol.*, 100 (2009) 1285–1290.
- [41] O. Ugurlu, J. Haus, A.A. Gunawan, M.G. Thomas, S. Maheshwari, M. Tsapatsis, K.A. Mkhoyan, Radiolysis to knock-on damage transition in zeolites under electron beam irradiation, *Phys. Rev. B*, 83 (2011) 113408.
- [42] Q. Zhu, Y.K. Sun, F.S. Na, J. Wei, S. Xu, Y.L. Li, F. Guo, Fabrication of CdS/titanium-oxo-cluster nanocomposites based on a Ti-32 framework with enhanced photocatalytic activity for tetracycline hydrochloride degradation under visible light, *Appl. Catal., B*, 254 (2019) 541–550.
- [43] J.B. Pan, J.J. Liu, H.C. Ma, S.L. Zuo, U.A. Khan, Y.C. Yu, B.S. Li, Structure of flower-like hierarchical CdS QDs/Bi₂WO₆ heterojunction with enhanced photocatalytic activity, *New J. Chem.*, 42 (2018) 7293–7300.
- [44] N. Li, Y. Tian, J.H. Zhao, J. Zhang, W. Zuo, L.C. Kong, H. Cui, Z-scheme 2D/3D g-C₃N₄@ZnO with enhanced photocatalytic activity for cephalixin oxidation under solar light, *Chem. Eng. J.*, 352 (2018) 412–422.
- [45] F. Chen, Q. Yang, X.M. Li, G.M. Zeng, D.B. Wang, C.G. Niu, J.W. Zhao, H.X. An, T. Xie, Y.C. Deng, Hierarchical assembly of graphene-bridged Ag₃PO₄/Ag/BiVO₄ (040) Z-scheme photocatalyst: an efficient, sustainable and heterogeneous catalyst with enhanced visible-light photoactivity towards tetracycline degradation under visible light irradiation, *Appl. Catal., B*, 200 (2017) 330–342.
- [46] J. Resasco, H. Zhang, N. Kornienko, N. Becknell, H. Lee, J.H. Guo, A.L. Briseno, P.D. Yang, TiO₂/BiVO₄ nanowire heterostructure photoanodes based on Type II band alignment, *ACS Cent. Sci.*, 2 (2016) 80–88.
- [47] C.R. Chen, H.Y. Zeng, M.Y. Yi, G.F. Xiao, R.L. Zhu, X.J. Cao, S.G. Shen, J.W. Peng, Fabrication of Ag₂O/Ag decorated ZnAl-layered double hydroxide with enhanced visible light photocatalytic activity for tetracycline degradation, *Ecotoxicol. Environ. Saf.*, 172 (2019) 423–431.
- [48] F. Chen, Q. Yang, J. Sun, F.B. Yao, S. Wang, Y.L. Wang, X.L. Wang, X.M. Li, C.G. Niu, D.B. Wang, G.M. Zeng, Enhanced photocatalytic degradation of tetracycline by Ag₂O/BiVO₄ heterojunction under visible-light irradiation: mineralization efficiency and mechanism, *ACS Appl. Mater. Interfaces*, 8 (2016) 32887–32900.
- [49] X.Z. Yuan, L.B. Jiang, J. Liang, Y. Pan, J. Zhang, H. Wang, L.J. Leng, Z.B. Wu, R.P. Guan, G.M. Zeng, *In-situ* synthesis of 3D microsphere-like In₂S₃/InVO₄ heterojunction with efficient photocatalytic activity for tetracycline degradation under visible light irradiation, *Chem. Eng. J.*, 356 (2019) 371–381.